



Available online at www.sciencedirect.com

ScienceDirect

Procedia Structural Integrity 53 (2024) 315-326



Third European Conference on the Structural Integrity of Additively Manufactures Materials (ESIAM23)

Experimental evaluation of the fatigue notch factor in as-built specimens produced by Wire and Arc Additive Manufacturing

E. Zancato^a, D. Leonetti^{a,*}, G. Meneghetti^b, J. Maljaars^{a,c}

^aEindhoven University of Technology, Department of the Built Environment, de Zaale - 5612 AZ Eindhoven, The Netherlands ^bUniversity of Padova, Department of Industrial Engineering, via Venezia 1 – 35131 Padova, Italy ^cTNO, Stieltjesweg 1 - 2628 CK Delft, The Netherlands

Abstract

The notch effects created by the rough surface of as-built Wire and Arc Additive Manufactured (WAAMed) products may negatively affect the fatigue resistance. This can be prevented by post-production treatments such as machining, but it implies an additional manufacturing step involving costs and time. There is a need to quantify the actual notch effects of as-built surfaces of WAAMed parts, which can be accomplished via a parameter called fatigue notch factor. This paper focuses on the experimental evaluation of the fatigue notch factor in as-built WAAMed specimens made of AISI 308LSi stainless steel tested with a load ratio of 0.1. Two test series consisting of as-built and machined plain specimens, respectively, have been tested by applying the load perpendicularly to the deposition plane. In this loading configuration, the as-built surface can be regarded as made of periodic notches. A dedicated specimen geometry based on the indications given in the International Standard ASTM E466-21 has been used for the tests. This innovative design allows to induce crack initiation in the periodic notches of the as-built surface while preventing the final fatigue fracture at the first notch root. After the fatigue tests, the fracture surfaces resulting from some specimens have been analyzed using the Scanning Electron Microscope (SEM) to determine the location of crack initiation. As a result of the study, the S-N curves in terms of nominal stress range have been derived and the fatigue notch factor has been determined.

© 2023 The Authors. Published by Elsevier B.V.

This is an open access article under the CC BY-NC-ND license (https://creativecommons.org/licenses/by-nc-nd/4.0) Peer-review under responsibility of the scientific committee of the ESIAM23 chairpersons

Keywords: WAAM; As-built surface; Notch effect; Stainless steel

1. Introduction

Additive manufacturing (AM) techniques are increasingly being used in various industrial sectors to produce metal components due to their numerous benefits. These benefits, outlined by Bandyopadhyay et al. (2022), include the ability to create components with unique structural and mechanical properties while reducing material usage. It is

^{*} Corresponding author. Tel.:+31-40-247-6173 *E-mail address*: d.leonetti@tue.nl

crucial to utilize the components in their original (referred as as-built) state to exploit the full potential of these technologies and minimize the need for post-production work. Conventional machining techniques, typically employed for post-processing operations, severely curtail the freedom of geometry of the components. Currently, it is not feasible to make efficient use of Wire and Arc Additive manufactured (WAAMed) components in their as-built form for structural applications because it is not known what effect the as-built surface has on the behaviour of the component, particularly in terms of fatigue life. WAAM components are constructed by overlapping multiple layers of material. As a result, especially in the case of a loading direction perpendicular to the deposition plane, the as-built surface can be compared to periodic notches. Notches significantly contribute to a reduction in the fatigue life of structural components, due to the fact that stresses concentrate at their root. The quantification of the effect of stress concentrators in terms of the theoretical stress concentration factor, k_t , is not sufficient to quantify the effect of the notch on the fatigue life, due to microstructural effects and statistical aspects Susmel (2022)) and the constraints of the most severely stressed regions. It is therefore necessary to evaluate and quantify the effect of the as-built surface on the fatigue life of WAAMed components. At present, there already exist some instances in the literature on the monotonic characterization of different materials fabricated through WAAM (Haden et al. (2017), Bercelli et al. (2021), Le et al. (2021), Li et al. (2021a), Li et al. (2021b), Tankova et al. (2022), Kotlarski et al. (2022), Müller et al. (2022), Shamir et al. (2022), Chernovol et al. (2023), Dağyıkan et al. (2023), Laghi et al. (2023)).

With regards to fatigue characterization, only a limited number of examples are available (Akgun et al. (2021), Bercelli et al. (2021), He et al. (2022), Shamir et al. (2022), Hensel et al. (2023), Huang et al. (2023), Ermakova et al. (2023), Leonetti et al. (2023)) and this number is further reduced when considering the effect of as-built surface notches on the fatigue strength of WAAMed components. The fatigue notch factor is a parameter that establishes a relation between the performance of a notched component - in this instance one containing an as-built surface - and the performance of a smooth component and it can be estimated using the following equation:

$$k_f = \frac{\Delta \sigma_{R,N,smooth}}{\Delta \sigma_{R,N,notched}} \tag{1}$$

where $\Delta \sigma_{R,N,smooth}$ and $\Delta \sigma_{R,N,notched}$ are the endurance limits of the smooth and notched specimens, respectively, for the same load ratio $R = \sigma_{min}/\sigma_{max}$. The endurance limit - better expressed as the stress at the transition between finite and near-infinite life - is assumed as the stress range corresponding to a fatigue life of $2 \cdot 10^6$ cycles. This value has been estimated by Hensel et al. (2023) for AM80 components produced by Direct Energy Deposition (DED), where k_f is estimated between 1.34 and 2.00 using specimens extracted in the direction perpendicular to the deposition plane. Values in a similar range, i.e. from 1.55 to 2.16, have been analytically evaluated by Huang et al. (2023) for a WAAMed thin-wall component made of ER70S-6.

In this research, the fatigue notch factor due to the as-built surface in stainless steel grade AISI 308 LSi WAAMed plates is evaluated through an experimental campaign consisting of fatigue tests conducted on specimens extracted from such plates, considering a load ratio R = 0.1. The uniaxial cyclic load has been applied normal to the deposition plane, as this direction is deemed to be the most critical (Leonetti et al. (2023)). A novel design of the specimens is presented, aiming to preserve the notch effect in as-built WAAM components. The design indicated in the standards has been developed for smooth components and do not take into account the effect of periodic notches on the components and the possible failure at the first notch. Furthermore, the research presents an analysis of the fracture surfaces of the broken specimens through an Scanning Electron Microscope (SEM) microscope.

2. Material and methods

Fatigue tests have been conducted on specimens extracted from WAAMed plates in order to experimentally determine the fatigue notch factor. The plates are produced by the company MX3D[©], and are shown in Figure 1. The plates HF1 and HF2 are used for the extraction of specimens for axial fatigue tests, see Figures 1a and 1b, respectively. Moreover, the plate T1, shown in Figure 1c, is used for the extraction of specimens for static tensile tests. Prior to conducting fatigue tests, the material has been characterized by means of tensile tests, hardness measurements, and metallographic investigations, described in Section 2.1. The design of the specimens and the test plan are described in 2.2, together with a description of the test setup.

specimens.

2.1. Mechanical properties and microstructure

specimens, isometric view.

The specimens used for the monotonic properties, hardness measurement, and microstructural investigation are extracted from the plate HF1. Three tensile test specimens and six metallographic analysis on samples have been extracted.



Fig. 1: Pictures of the WAAMed plates

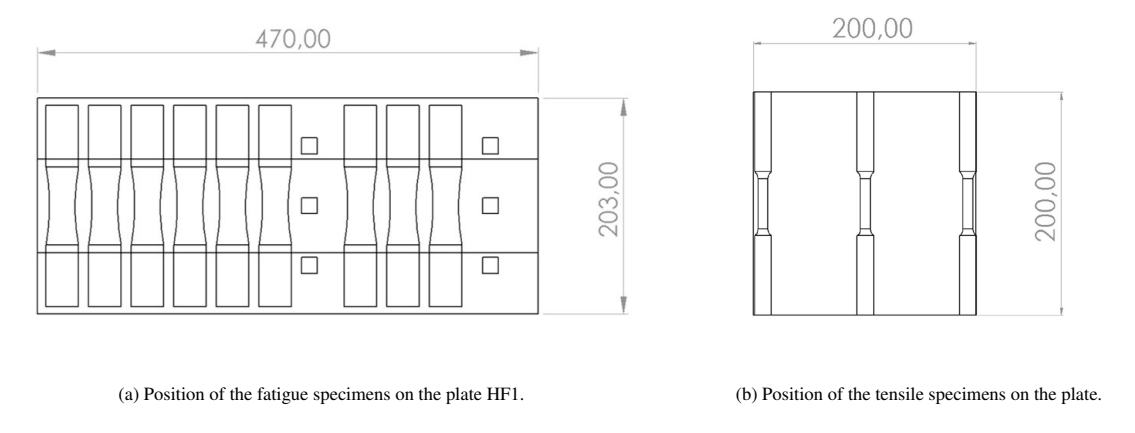


Fig. 2: Drawings of the WAAMed plates

The metallographic analysis is carried out first, where the six samples are extracted by waterjet cutting from plate HF1. Waterject cutting was used to minimize the induced heat. The position of the samples is illustrated in Figure 2a. The extraction of samples from both the center and the side of the plate allows to study any variation in the microstructure within the plate that can be due to the different cooling conditions of the layers. For each of the three sets of samples a different surface was examined under an optical $Leica\ DMRE$ microscope, following the instructions in the standard ASTM-E3 ASTM (2011). The surfaces have been named with the letters D,E,F and are shown in Figure 3. The rolling direction indicated in the ASTM E3 standard is replaced with the direction of the weld beads on the deposition plane in this study. After the preparation of the samples, consisting of grinding and polishing procedures, they have been etched with a compound consisting of 10% aqueous oxalic acid ($HO_2C - CO_2H$), where a current with a voltage of 6V was passed through and the immersion lasted for about 30 s. Afterwards, the components have been analysed under the optical microscope.

From one of the tested samples, characterized by an analysis surface parallel to the as-built surface, nine Vickers microhardness measurements are taken using a *Shimadorii 95032* Vickers hardness tester, with a weight of 0.1 kg and an indentation time of 15 s.

The monotonic static tensile tests are conducted with an *Instron 5985* universal testing machine having a capacity of 250 kN, and equipped with a force transducer of the same nominal capacity. The elongation is monitored using an AVE2 optical extensometer, considering an initial gauge length of 40 mm. The tests are conducted by controlling the displacement of the cross-head of the machine, which is assigned a constant rate of 0.6 mm/min. The signals from the force transducer and the extensometer are sampled at a frequency of 300 samples/s by the controller. The design of the specimens is shown in Figure 3b, where the main dimensions are given in accordance with the ASTM (2021) standard. The dimensions are measured for each specimen and summarised in Table 1.

Table 1: Parameters	used for static	tensile tests	dimensions	illustrated in	Figure 3

	Specimen 1	Specimen 2	Specimen 3	unit
d	9.05	9.00	9.00	[mm]
G	40.33	40.48	39.82	[mm]
A	45	45	45	[mm]
Speed	0.6	0.6	0.6	[mm/min]

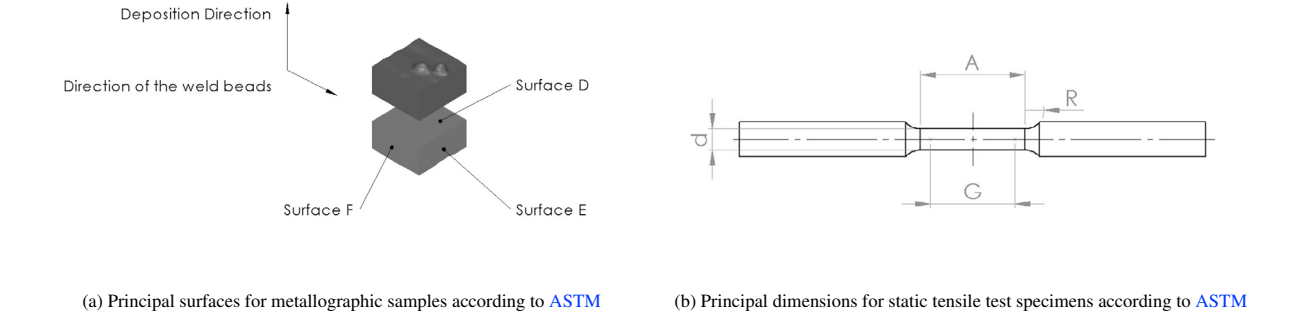


Fig. 3: Schematic representation of a metallographic sample and a static tensile specimen

2.2. Fatigue tests

The uniaxial fatigue tests have been conducted on a *Schenck* hydraulic testing machine having a capacity of $400 \, \text{kN}$ and equipped with self-centering mechanical wedge grips. The tests are carried out considering a nominal stress range varying between 140 and 460 MPa, at a constant frequency of 7 Hz and a load ratio of R = 0.1.

A specimen design has been developed for the execution of fatigue tests on the notched components. This design conforms to the ASM International (2021) and ISO 1099:2006 (2006) guidelines whilst simultaneously introducing a variation to the shape of the specimen. The standard practice involves using an hourglass-shaped test piece with a rectangular cross-section and uniform thickness. However, for preserving the as-built surface, the conventional hourglass geometry may not provide sufficient resistance at the grip section. Crack nucleation can result at the root of the first notch of the as-built surface due to the fact the grip section of the specimens needs to be machined, in order to place the specimen in the testing machine. This happens because the first and the last notches in periodic notches are characterized by higher stress concentration as compared to the others, creating what is referred to as the *first notch effect*. This effect has mainly been characterised for bolted connections, where the threads are considered as a set of notches in series (Fukuoka et al. (1985)), but is in general applicable for periodic notches. To prevent this effect and to ensure that crack nucleation occurs in the central section, the plates have been produced with an hourglass shape, see Figure 1a, taking advantage of the opportunities offered by WAAM. This allows the hourglass shape to be used for both the front and the lateral plane of the specimen, as depicted in Figure 4a.

In addition, the dimensions of the specimen are such that the grip area is 1.5 times larger than the minimum area in the central section. Therefore, failure is expected in the central portion of the specimen.

Two categories of samples are established: (1) specimens of type A, which feature two as-built surfaces (Fig. 4b), and (2) specimens of type B (Fig. 4c), which are produced from fully machined type A specimens.

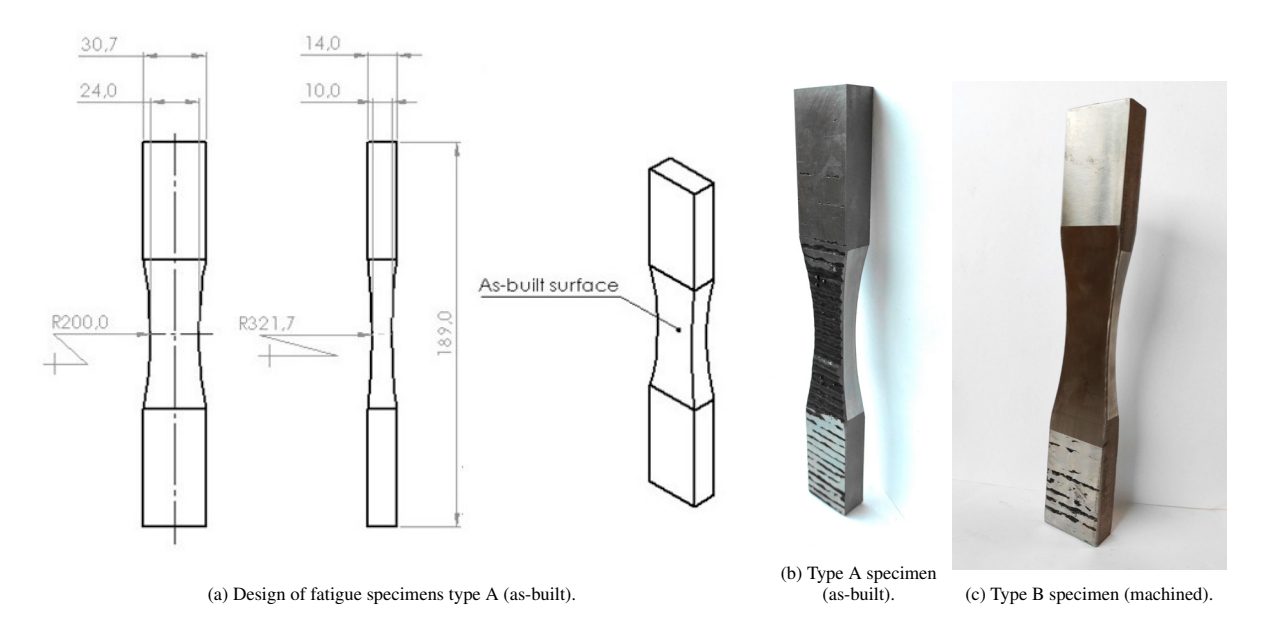


Fig. 4: Uniaxial fatigue specimens

Once attained their final shape, the specimens were measured with a caliper to obtain the width and thickness of the grip area and the central portion. For measuring the thickness at the center of the specimens, a caliper is positioned perpendicularly to the longitudinal axis of symmetry of the specimen. Three measures are taken while the edges of the caliper touch different points in the valleys of the weld beads. The thickness of the specimen is then obtained as the average of the three readings. Table 3 reports the dimensions of the specimens. As the table shows, two nominal dimensions are selected for the width of the specimens, namely 18 and 24 mm. The latest specimens, i.e. from Specimen 9 onward, had a larger width to ensure sufficient grip in the machine also at low load levels.

3. Experimental results

This section presents the results of the experimental campaign.

3.1. Mechanical properties and microstructure

The micrographs obtained from the microscopic analysis are illustrated in Figure 5a, 6a and 7a. They show a clear change in microstructure at the weld bead observation point, where coarse grains, containing δ -ferrite with both lacy and vermicular morphology, transit to fine columnar grains. The changes in texture in the microstructure are the cause of the anisotropy of the material, whose evaluation is currently under investigation. In this study, grains are shown to be elongated and oriented parallel to the building direction, which is in agreement with other studies, see (Haden et al. (2017), Ge et al. (2018)). From a global perspective, the material shows no significant defects, with the exception of some porosity, which can be explained by the lack of cleaning between layers, as indicated by Queguineur et al. (2018) for AISI 316L. The small number of pores present allows for classifying this material as 'low defect', as outlined by Ge et al. (2018) and Haden et al. (2017).

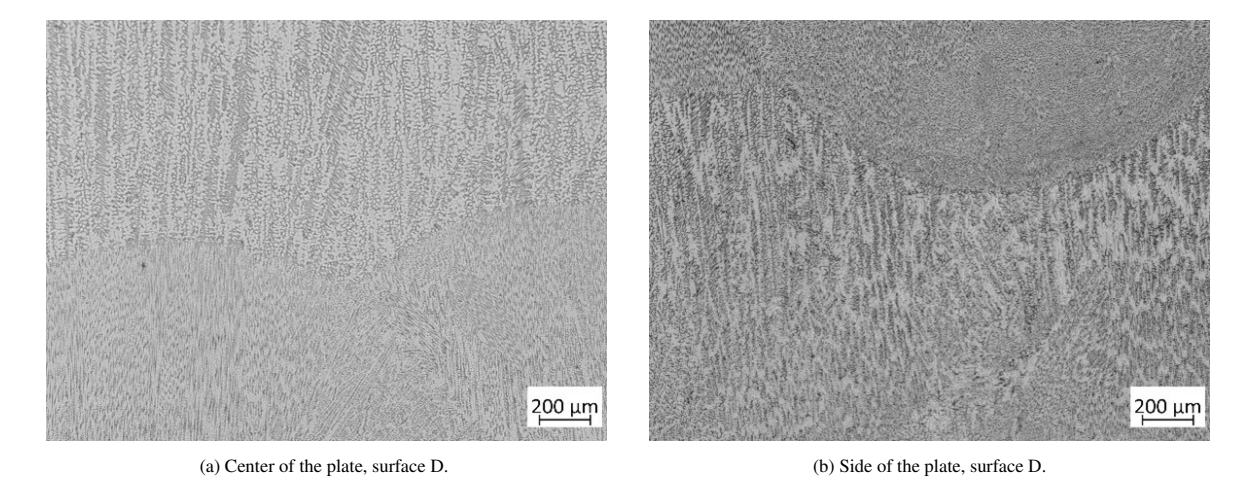


Fig. 5: Micrographs of metallographic samples where surface D was analysed

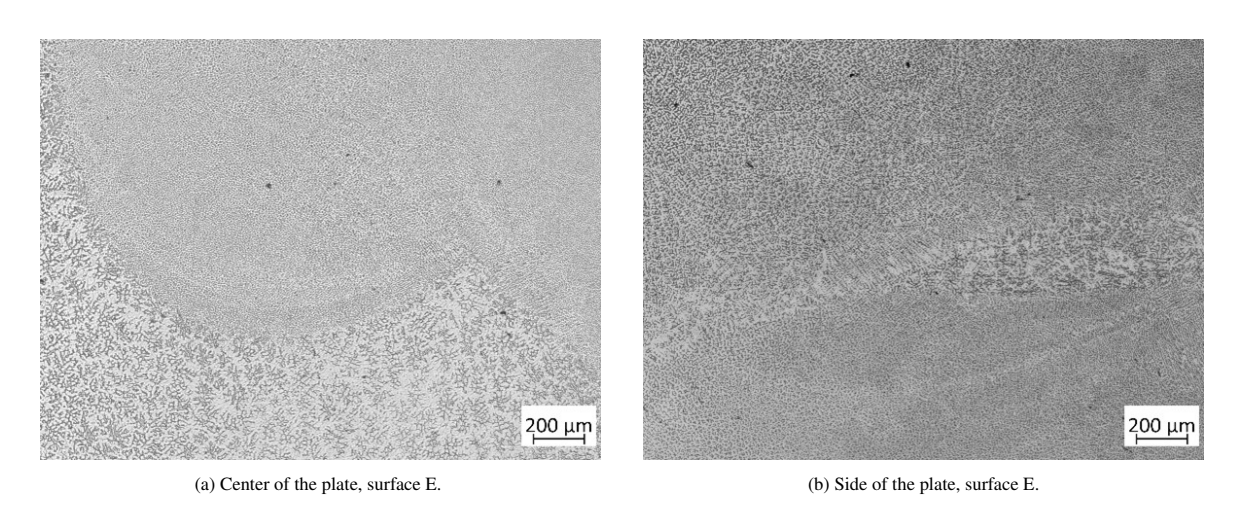


Fig. 6: Micrographs of metallographic samples where surface E was analysed

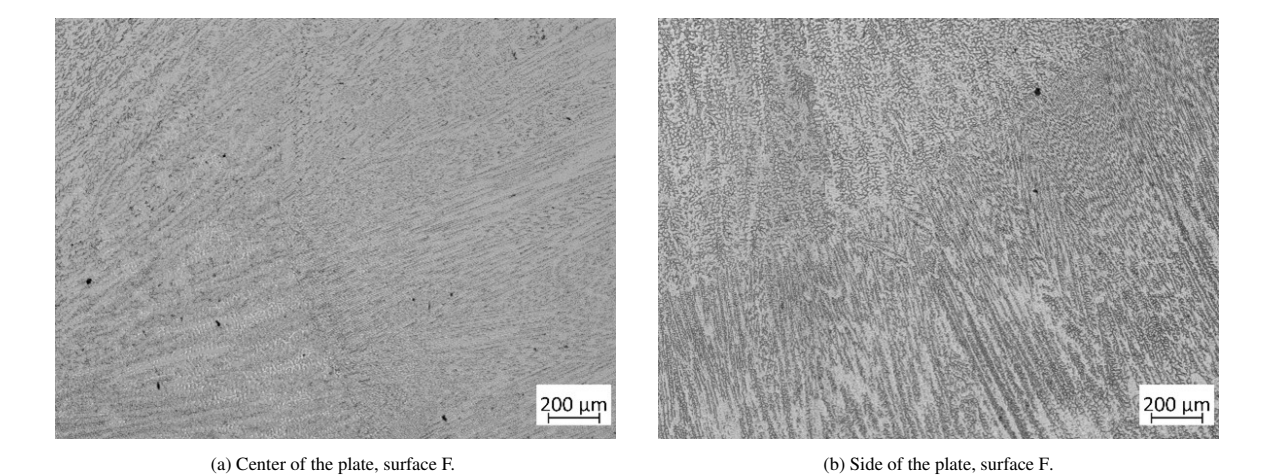


Fig. 7: Micrographs of metallographic samples where surface F was analysed

Further characteristics of the material are inferred from the tensile and hardness test results, which are illustrated in the Table 2.

σ_P	σ_Y	σ_U	E	HV
[MPa]	[MPa]	[MPa]	[GPa]	[HV]
206.14 ± 11.64	304.66 ± 6.78	531.94 ± 4.45	114.23 ± 1.10	165.7 ± 1.51

Table 2: Mechanical properties of WAAMed 308LSi.

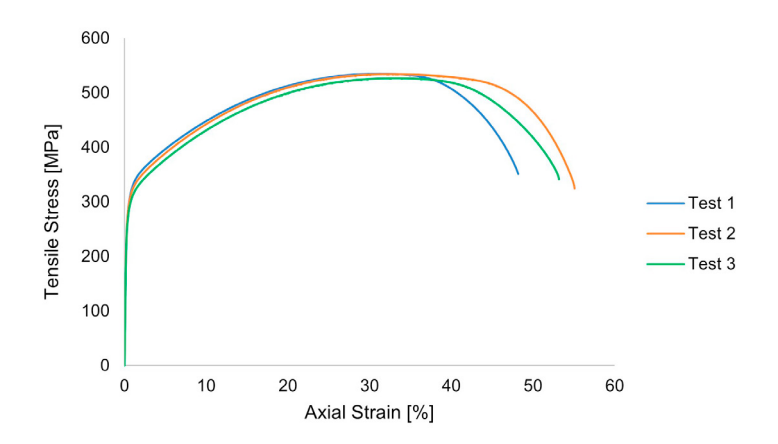


Fig. 8: Stress-strain curves for WAAMed 308LSi.

As evidenced from Figure 8 and well known from other tests on the same alloy, the material does not exhibit a yield plateau. The yield stress, σ_Y in Table 2, is therefore taken as the 0.2% proof stress using the "Offset method" according to the ASTM (2021). Moreover, the elastic proportionality limit, σ_P , is approximately 100 MPa lower than the yield stress. The tensile strength σ_U is approximately 75% higher than the yield stress. The ratio between Vickers hardness HV and tensile strength is as expected. Overall, the observed mechanical properties for this material are consistent with those found by Laghi et al. (2023) and Leonetti et al. (2023), with the exception of a slightly lower value of elastic modulus, E.

3.2. Fatigue tests

The specimen dimensions, test conditions and the results of the fatigue tests are reported in Table 3 and Table 4. In the tables, the main dimensions of the test specimen are presented, i.e. the width and thickness of the centre and grip section (w, t, W and T, respectively) and the ratio of grip area to centre section area, $\frac{A_{grip}}{A_{neck}}$. Then, the main test parameters are presented, i.e. frequency f, nominal stress range $\Delta \sigma$, and number of cycles N. The last column is dedicated to the indication of failure: $\delta = 1$ means that the specimen has reached the end of its life, i.e. complete separation occurred; On the other hand, $\delta = 0$ means that the specimen has not broken at $2 \cdot 10^6$ cycles and is considered as a right censored data.

On the basis of these results, S-N curves have been determined following the Basquin equation:

$$log_{10}(N) = m \cdot log_{10}(\Delta\sigma) + a \tag{2}$$

where $log_{10}(\Delta\sigma)$ is the independent variable, $log_{10}(N)$ is the dependent variable, m is the negative inverse slope of the S-N curve, and a is the intercept parameter of the curve. The least square method has been used to estimate the parameters of the curve, i.e. \hat{a} and \hat{m} . The specimens that did not fail are disregarded. Therefore, the estimators of

Spec	w	t	W	T	$\frac{A_{grip}}{A_{neck}}$	f	$\Delta \sigma$	N	δ
	[mm]	[mm]	[mm]	[mm]	[]	[Hz]	[MPa]	[cycles]	
1	18.2	9.52	26.6	13.8	2.12	7	316	10641	1
2	18.0	9.31	26.6	13.8	2.19	7	285	27860	1
3	18.1	9.40	26.6	13.8	2.16	7	256	39328	1
4	17.9	9.30	26.4	13.8	2.19	7	229	85926	1
5	17.9	9.15	26.4	13.8	2.22	7	207	146849	1
9	24.1	10.1	30.9	13.8	1.75	7	180	116195	1
10	24.1	9.94	30.8	13.8	1.78	7	18	215441	1
11	24.0	9.69	30.9	13.9	1.84	10	160	259619	1
12	24.2	9.73	30.9	13.9	1.82	10	160	275082	1
13	24.1	9.65	30.8	13.8	1.83	10	140	2000000	0
14	24.1	9.88	30.6	13.9	1.79	10	140	826037	1
21	24.1	9.82	30.8	13.8	1.80	7	300	21947	1
22	24.0	9.57	30.8	13.8	1.85	7	250	55699	1

Table 3: Results of the fatigue axial tests for type A specimens and R = 0.1.

Table 4: Results of the fatigue axial tests for type B specimens and R = 0.1.

Spec	w	t	W	T	$\frac{A_{grip}}{A_{neck}}$	f	$\Delta \sigma$	N	δ
	[mm]	[mm]	[mm]	[mm]		[Hz]	[MPa]	[cycles]	
1	24.0	6.97	30.8	13.9	2.55	7	300	483948	1
2	24.2	6.99	30.7	13.9	2.52	7	400	90580	1
3	23.9	6.95	30.9	14.1	2.61	7	320	265773	1
4	24.2	6.95	30.8	13.9	2.56	7	420	62798	1
5	24.2	6.96	30.9	13.9	2.57	7	440	51996	1
6	24.2	7.05	30.7	13.9	2.50	7	460	34279	1
7	24.2	6.98	30.7	13.9	2.55	7	280	2000000	0
8	24.0	7.02	30.9	14.02	2.57	7	360	201031	1

the parameters and the standard deviation on the number of cycles σ_{logN} , have been calculated as indicated by Khuri (2013):

$$\hat{m} = \frac{\sum (log_{10}(\Delta\sigma_i) - E[log_{10}(\Delta\sigma)]) \cdot (log_{10}(N_i) - E[log_{10}(N)])}{\sum (log_{10}(\Delta\sigma_i) - E[log_{10}(\Delta\sigma)])^2}$$
(3)

$$\hat{a} = E[\log_{10}(N)] + \hat{m} \cdot E[\log_{10}(\Delta\sigma)] \tag{4}$$

$$\hat{\sigma}_{logN} = \sqrt{\frac{\sum (log_{10}(N_i) - (\hat{a} + \hat{m} \cdot log_{10}\Delta\sigma_i))}{n_s - 2}}$$
(5)

where E[] denotes the expectation operator, \hat{m} and \hat{a} are the estimators of the parameters of the S-N curve, and n_s is the number of failed specimens. The S-N curves and the test data are depicted in Figure 9. The estimators of the parameters of the S-N curves are reported in Table 5 for both test series. The negative inverse slope parameters of the two curves are $\hat{m} = 4.21$ for Type A specimens and $\hat{m} = 5.88$ for Type B specimens. The inverse slope determined for components including as-built surfaces, which aligns with findings from comparable materials in other studies (Hensel et al. (2023)), is similar to that of welded components, where the crack growth is more significant than the initiation stage. On the other hand, the results obtained for fully machined specimens indicate a larger importance of the initiation phase and possibly a more dominant effect of plasticity on the crack nucleation point.

Table 5: Parameters of median the S-N curves resulting from the test series

Series	ĥ	â	$\hat{\sigma}_{logN}$
Type A	4.21	14.78	0.12
Type B	5.88	20.24	0.06

An estimate of the fatigue notch factor according to Equation 1 is derived from the S-N curves of the Type A and Type B specimens. However, the ratio of fatigue strength between the two types depends on the stress range because of the different slope parameters. The fatigue notch factor k_f at $2 \cdot 10^6$ cycles is equal to 2.27.

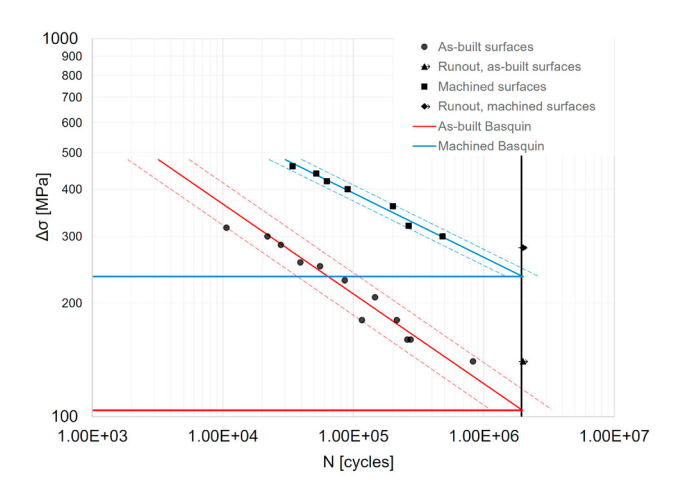
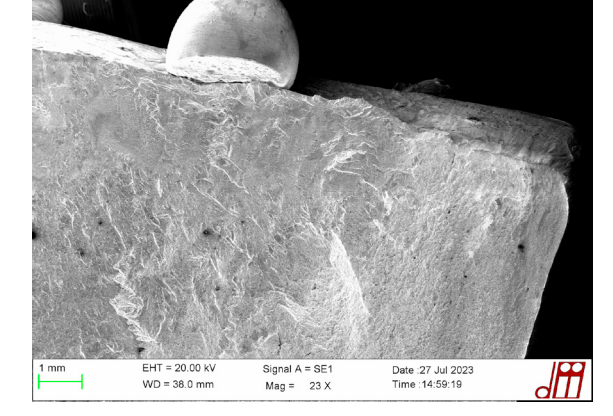


Fig. 9: Comparison between the S-N curves used for the experimental estimation of the fatigue notch factor for $2*10^6$ cycles.

3.3. Analysis of the fracture surfaces

Some of the broken samples have been examined with Zeiss Evo Ma10 SEM to identify the location of crack initiation, either from internal material defects - although these are not revealed by the metallography - or from the as-built surface. The analyses indicate that the dominant final fatigue crack is formed after the coalescence of multiple cracks emanating from the as-built surface (Figure 10). The occurrence of weld spatter at the surface, as shown in Figure 10b, appears to have no impact on the crack initiation, whilst irregularities like deep valleys, as shown in Figure 12. These defects are not present in fully machined components and, considering the absence of significant internal defects, the crack initiation of these components is attributed to initiation of corner cracks, developed from the sharp edges of the specimens despite the smoothing process performed on them.

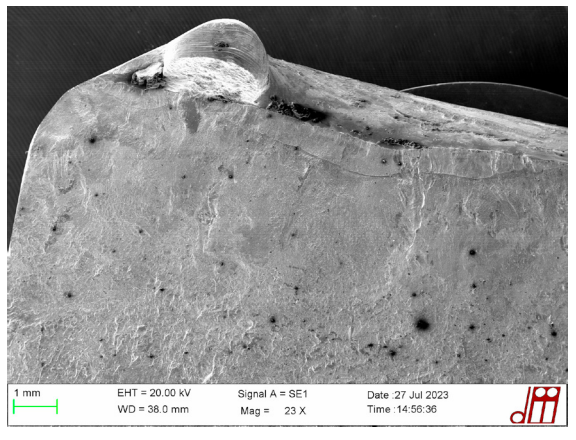


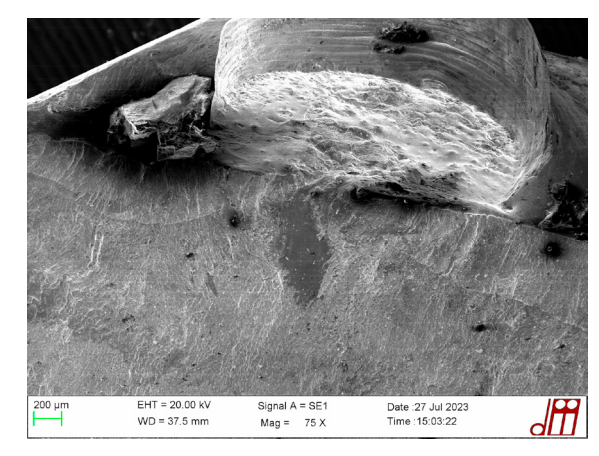


(a) Surface fracture of specimen A14.

(b) Zoom of the fracture surface of specimen A14.

Fig. 10: SEM analysis of specimen 14.

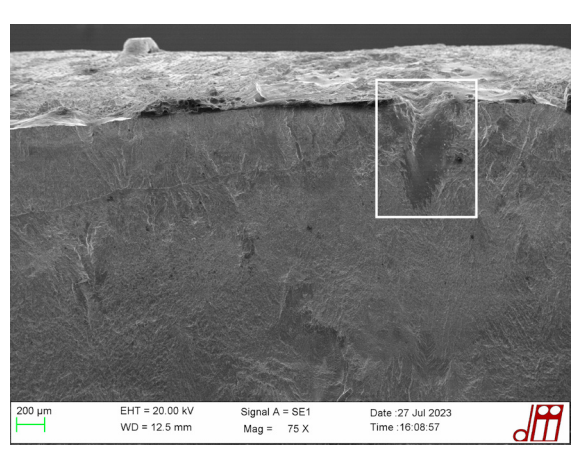


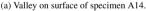


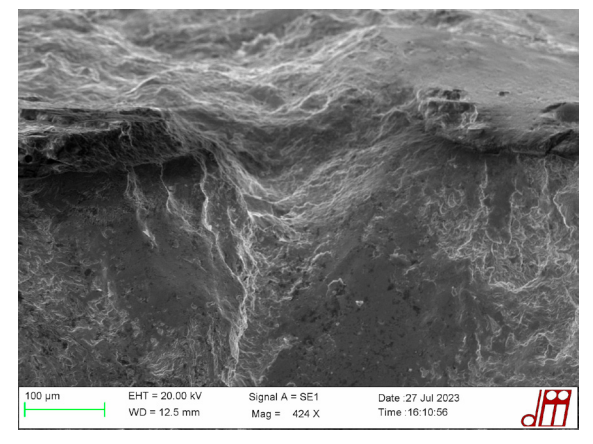
(a) Multiple cracks propagating from as-built surface of specimen A14.

(b) Zoom of a spatter present on specimen A14.

Fig. 11: SEM analysis of specimen 14.







(b) Zoom of the valley present on specimen A14.

Fig. 12: SEM analysis of specimen 14.

4. Conclusions

This paper presented an experimental investigation regarding the fatigue strength of WAAM 308LSi, with emphasis on the effect of the as-built surface. This has been quantified in terms of fatigue notch factor by a comparison of the S-N curves of specimens with machined (Type B) and as-built (Type A) surfaces. The fatigue tests have been conducted on specimens with a specific design at a load ratio R=0.1 resulting in S-N curves characterized by a negative inverse slope of 4.21 and 5.88 for Type A and B, respectively. These values denote that both crack initiation and crack growth mechanisms contribute to the fatigue life, with crack initiation being more relevant for smooth specimens with machined surfaces. The fatigue notch factor at 2 million cycles has been estimated as 2.27.

The investigation of the microstructure shows a transition from coarse grains, containing δ -ferrite with both lacy and vermicular morphology, to fine columnar grains at the weld bead. These grains are elongated and oriented parallel to the building direction, in agreement with other studies.

The analysis of fracture surfaces from specimens with as-built surfaces indicates that the fracture is due to periodic notches and surface defects. Any significant internal defects were not found in the analyzed samples.

Acknowledgements

The authors would like to acknowledge Jean-François Moulin and MX3D©for the material provided and Mark Luijbregts from LEC3D©for his support. The activities have been part of the project "The strength of additive manufactured metals against fatigue" financed by Boost!, provided by Eindhoven University of Technology.

References

- Akgun, E., Zhang, X., Biswal, R., Zhang, Y., Doré, M., 2021. Fatigue of wire+arc additive manufactured Ti-6Al-4V in presence of process-induced porosity defects. International Journal of Fatigue 150. doi:10.1016/j.ijfatigue.2021.106315.
- ASM International, 2021. E466-2021 Standard practice for conducting force controlled constant amplitude axial fatigue tests of metallic materials. ASTM International, West Conshohocken, PA.
- ASTM, 2011. E3-11 Standard Guide for Preparation of Metallographic Specimens 1. ASTM Copyright. i. doi:10.1520/E0003-11.2.
- ASTM, 2013. Standard Terminology Relating to Fatigue and Fracture Testing ASTM Designation E1823-13. Annual Book of ASTM Standards 03
- ASTM, 2021. ASTM E8/E8M standard test methods for tension testing of metallic materials. Annual Book of ASTM Standards .
- Bandyopadhyay, A., Traxel, K.D., Lang, M., Juhasz, M., Eliaz, N., Bose, S., 2022. Alloy design via additive manufacturing: Advantages, challenges, applications and perspectives. doi:10.1016/j.mattod.2021.11.026.
- Bercelli, L., Moyne, S., Dhondt, M., Doudard, C., Calloch, S., Beaudet, J., 2021. A probabilistic approach for high cycle fatigue of Wire and Arc Additive Manufactured parts taking into account process-induced pores. Additive Manufacturing 42. doi:10.1016/j.addma.2021.101989.
- Chernovol, N., Marefat, F., Lauwers, B., Van Rymenant, P., 2023. Effect of welding parameters on microstructure and mechanical properties of mild steel components produced by WAAM. Welding in the World 67. doi:10.1007/s40194-022-01422-1.
- Dağyıkan, K., Gürol, U., Koçak, M., 2023. Characterization and fracture toughness evaluation of the thick-walled wire arc additively manufactured low alloy steels. Welding in the World 67. doi:10.1007/s40194-022-01424-z.
- Ermakova, A., Razavi, N., Berto, F., Mehmanparast, A., 2023. Uniaxial and multiaxial fatigue behaviour of wire arc additively manufactured ER70S-6 low carbon steel components. International Journal of Fatigue 166. doi:10.1016/j.ijfatigue.2022.107283.
- Fukuoka, T., Yamasaki, N., Kitagawa, H., Hamada, M., 1985. STRESS ANALYSIS OF THREADED PORTIONS IN FASTENING. Bulletin of the JSME 28. doi:10.1299/jsme1958.28.2247.
- Ge, J., Lin, J., Chen, Y., Lei, Y., Fu, H., 2018. Characterization of wire arc additive manufacturing 2Cr13 part: Process stability, microstructural evolution, and tensile properties. Journal of Alloys and Compounds 748. doi:10.1016/j.jallcom.2018.03.222.
- Haden, C.V., Zeng, G., Carter, F.M., Ruhl, C., Krick, B.A., Harlow, D.G., 2017. Wire and arc additive manufactured steel: Tensile and wear properties. Additive Manufacturing 16. doi:10.1016/j.addma.2017.05.010.
- He, J., Feng, X., Wang, X., Guan, X., 2022. Fatigue performance and acoustic emission behavior of remanufactured low-carbon steel made by wire and arc additive manufacturing. International Journal of Fatigue 165. doi:10.1016/j.ijfatigue.2022.107190.
- Hensel, J., Müller, J., Scharf-Wildenhain, R., Uhlenberg, L., Hälsig, A., 2023. The effects of building position on surface and fatigue of DED-arc steel components. Welding in the World 67. doi:10.1007/s40194-022-01431-0.
- Huang, C., Li, L., Pichler, N., Ghafoori, E., Susmel, L., Gardner, L., 2023. Fatigue testing and analysis of steel plates manufactured by wire-arc directed energy deposition. Additive Manufacturing 73. doi:10.1016/j.addma.2023.103696.
- ISO 1099:2006, 2006. Metallic materials. Fatigue testing. Axial force-controlled method. International Organization for Standardization, Geneva, Switzerland 10992006.
- Khuri, A.I., 2013. Introduction to Linear Regression Analysis, Fifth Edition by Douglas C. Montgomery, Elizabeth A. Peck, G. Geoffrey Vining. International Statistical Review 81. doi:10.1111/insr.12020{_}10.
- Kotlarski, G., Ormanova, M., Ossenbrink, R., Nikitin, A., Doynov, N., Valkov, S., Michailov, V., 2022. Fabrication and Characterization of Wire Arc Additively Manufactured AlSi5 Structures. Metals 12. doi:10.3390/met12111870.
- Laghi, V., Arrè, L., Tonelli, L., Di Egidio, G., Ceschini, L., Monzón, I., Laguía, A., Dieste, J.A., Palermo, M., 2023. Mechanical and microstructural features of wire-and-arc additively manufactured carbon steel thick plates. International Journal of Advanced Manufacturing Technology 127. doi:10.1007/s00170-023-11538-3.
- Le, V.T., Mai, D.S., Doan, T.K., Paris, H., 2021. Wire and arc additive manufacturing of 308L stainless steel components: Optimization of processing parameters and material properties. Engineering Science and Technology, an International Journal 24. doi:10.1016/j.jestch. 2021.01.009.
- Leonetti, D., de Munnik, M., Kassing, L., Khan, D., Moulin, J.F., Snijder, B., 2023. Rotating bending fatigue behaviour and quasi-static tensile properties of Wire Arc Additively Manufactured 308L stainless steel. ce/papers 6, 732-738. URL: https://onlinelibrary.wiley.com/doi/abs/10.1002/cepa.2441, doi:https://doi.org/10.1002/cepa.2441.
- Li, K., Klecka, M.A., Chen, S., Xiong, W., 2021a. Wire-arc additive manufacturing and post-heat treatment optimization on microstructure and mechanical properties of Grade 91 steel. Additive Manufacturing 37. doi:10.1016/j.addma.2020.101734.
- Li, Y., Wu, S., Li, H., Dong, Y., Cheng, F., 2021b. Submerged arc additive manufacturing (SAAM) of low-carbon steel: Effect of in-situ intrinsic heat treatment (IHT) on microstructure and mechanical properties. Additive Manufacturing 46. doi:10.1016/j.addma.2021.102124.
- Müller, J., Hensel, J., Dilger, K., 2022. Mechanical properties of wire and arc additively manufactured high-strength steel structures. Welding in the World 66. doi:10.1007/s40194-021-01204-1.

- Queguineur, A., Rückert, G., Cortial, F., Hascoët, J.Y., 2018. Evaluation of wire arc additive manufacturing for large-sized components in naval applications. Welding in the World 62. doi:10.1007/s40194-017-0536-8.
- Shamir, M., Igwemezie, V., Lotfian, S., Jones, R., Asif, H., Ganguly, S., Mehmanparast, A., 2022. Assessment of mechanical and fatigue crack growth properties of wire + arc additively manufactured mild steel components. Fatigue and Fracture of Engineering Materials and Structures doi:10.1111/ffe.13797.
- Susmel, L., 2022. Notches, nominal stresses, fatigue strength reduction factors and constant/variable amplitude multiaxial fatigue loading. International Journal of Fatigue 162. doi:10.1016/j.ijfatigue.2022.106941.
- Tankova, T., Andrade, D., Branco, R., Zhu, C., Rodrigues, D., Simões da Silva, L., 2022. Characterization of robotized CMT-WAAM carbon steel. Journal of Constructional Steel Research 199. doi:10.1016/j.jcsr.2022.107624.